# The Faraday instability in miscible fluid systems

S.V. Diwakar, Farzam Zoueshtiagh, Sakir Amiroudine, Ranga Narayanan

# The Faraday instability in miscible fluid systems

Cite as: Phys. Fluids **27**, 084111 (2015); https://doi.org/10.1063/1.4929401
Submitted: 20 March 2015 • Accepted: 27 July 2015 • Published Online: 26 August 2015

S. V. Diwakar, Farzam Zoueshtiagh, Sakir Amiroudine, et al.

PHYSICS OF FLUIDS **27**, 084111 (2015)

# The Faraday instability in miscible fluid systems

S. V. Diwakar,[1,a)] Farzam Zoueshtiagh,[1,b)] Sakir Amiroudine,[2,c)] and Ranga Narayanan[3,d)]
[1]*Institut d'Electronique, de Microélectronique et de Nanotechnologie (IEMN) UMR CNRS 8520, Avenue Poincaré, Villeneuve d'Ascq 59652, France*
[2]*Institut de Mécanique et d'Ingénierie-TREFLE, University of Bordeaux, UMR CNRS 5295,16 Avenue Pey-Berland, Pessac Cedex 33607, France*
[3]*Department of Chemical Engineering, University of Florida, Gainesville, Florida 32611, USA*

(Received 20 March 2015; accepted 27 July 2015; published online 26 August 2015)

The Faraday instability arising in distinct miscible fluid layers, when the parametric forcing is parallel to the gravity vector, is analysed. A time-dependent density gradient is established from the moment the fluid layers are placed in contact with one another. The operating parameters in a miscible Faraday system are the frequency of parametric forcing and the wait time between the initial contact of fluids and the commencement of oscillations. Using a linearized theory that invokes a quasi-steady approximation, the vibrational threshold required for the onset of Faraday instability is evaluated for these parameters and several observations are made. First, the criticality is observed to occur at a sub-harmonic frequency. Second, the large magnitude of the concentration gradient at early wait times is found to make the thin layers highly unstable. Third, the stability increases with forcing frequency, owing to the increased dissipation of the resulting choppy waves. All these observations qualitatively agree with experiments. Finally, a calculation reveals that an increase in gravity increases the critical wavelength of flow onset and results in the reduction of critical input acceleration. © *2015 AIP Publishing LLC.* [http://dx.doi.org/10.1063/1.4929401]

## I. INTRODUCTION

The onset of flow patterns in density-stratified fluid layers, subject to parametric forcing, is known as the Faraday instability phenomenon.[1,2] Ordinarily, for this onset to occur from an erstwhile quiescent state, the forcing must act parallel to the density stratification. While the Faraday instabilities can generally occur in both miscible and immiscible fluid layers, the phenomena owe their origins to different hydrodynamic and transport mechanisms. In the case of immiscible liquids, the destabilization of the static layers is manifested by the transverse variation in interfacial elevation and occurs due to the resonance between the imposed frequency and the natural frequency of the system. The latter depends on the density difference as well as the surface tension and viscosities of the layers. The surface tension and viscous dissipation effects stabilize all the perturbations below a critical limit of the oscillation parameter. Beyond this limit, interfacial deformation takes the shape of a standing wave with a defined wavelength.

The density stratification in miscible fluid systems is generally caused by either temperature or solutal gradients. Where temperature differences are imposed, the temperature gradient, and therefore, density gradients, may either be steady or unsteady in time. However, in the case of solutal mass transfer, the solutal concentration differences are typically not constant in time and the

a)Electronic mail: Diwakar.Seyyanur-Venkatesan@iemn.univ-lille1.fr
b)Electronic mail: farzam.zoueshtiagh@univ-lille1.fr
c)Electronic mail: sakir.amiroudine@u-bordeaux.fr
d)Electronic mail: ranga@ufl.edu

 

density gradients are thus transient. The Faraday instability in such miscible fluid layers is distinct from the immiscible fluid layer case, as it is triggered by the transverse variation of fluid density and is countered by the stabilizing viscous and diffusion processes. Here too, the instability is a consequence of the resonance between the imposed and natural frequencies of the system. The mixing of fluids generated during the evolution of the instability gradually reduces the gradients of concentration in the layers and even results in the eventual "quenching" of the instability.[3,4] Thus, the Faraday instability in miscible systems has a definite lifespan which is determined by the different fluid properties and operating parameters and it sows the seeds of its own destruction.

The inherent transient nature of the diffusion process implies that the critical parameters for flow onset depend on the time delay between the commencement of oscillations and the moment the two fluid layers are brought into contact with one another—this is the so-called "wait–time," $t_0$. As the thickness of the diffusion layer is determined by the value of $t_0$, a smaller $t_0$ would generally imply large solutal gradients and thin layers. The former is destabilizing and the latter is stabilizing. Large values of $t_0$ lead to the reverse situation. Understanding the effect of the initiation time is therefore an important focal point of the current study. Notwithstanding the transient base state, the mechanisms of instability in the miscible Faraday problem are similar to those of the stably stratified vibrational Rayleigh-Bénard system.[5,6] For example, the frequency of system response is observed to be half of the imposed excitation frequency, a fact that is supported by the experimental observations of Zoueshtiagh *et al*.[3] Despite this similarity, the miscible Faraday system has not received as much theoretical scrutiny as its Bénard counterpart or as miscible systems with oscillations parallel to the interface.[7,8] The current work thus focusses on predicting the threshold for the onset of instability through a linear analysis. Aside of the scientific interest, the present work is also motivated by the profound impact which Faraday instabilities have on practical applications such as atomization and mixing of liquids.[9]

A general linear stability analysis of miscible systems is complicated by two significant challenges. First, the base state of the problem is transient and the corresponding linear system ceases to be of classical Floquet type. However, consideration of a frozen-time approximation wherein the base concentration profile is assumed to remain frozen during the evolution of the instability allows the resulting linear stability analysis to become fully amenable to the Floquet theory. The frozen-time approximation has been previously used for other hydrodynamic instability problems (cf. Riaz *et al*.[10] and Gresho and Sani[5]). Second, the spatial discretization of variables through Lagrangian interpolation polynomials at the Gauss-Lobatto-Chebyshev (G-L-C) points leads to an undesirable distribution of nodal points in the diffusion layer. Owing to its distribution pattern (finer near the extremities and coarser at the center), the G-L-C points do not properly resolve the mixing region present in the domain. This consequently leads to large errors in the predicted critical parameters as the sharp gradients in the diffusion region are poorly approximated. As a remedy, a mapping procedure is adopted here that allows for clustering of nodes around the diffuse interface in the physical domain. Spectrally accurate solutions are then obtained by mapping the clustered nodes onto the G–L–C points in the computational domain. The aim of the current work is to predict the threshold of the miscible Faraday instability for different operating conditions. To this end, we now describe the mathematical model and its implementation.

## II. MATHEMATICAL MODEL

Consider two layers of miscible fluids, enclosed between two infinite horizontal plates, as shown in Fig. 1, with gravity acting in the downward vertical direction. When the layers first come into contact, a transiently growing diffuse region of thickness $L(t)$ is formed along their location of initial contact owing to the continuous mass diffusion process in the vertical $y$-direction. We shall hereafter refer to this transient diffuse region as the "mixing region" and the initial contact location as the "diffuse interface". The general unscaled equation governing the evolution of fluid concentration in the domain under non-flow conditions is given by

$$\left(\frac{\partial C_0}{\partial t}\right) = D\left[\frac{\partial^2 C_0}{\partial y^2}\right], \tag{1}$$

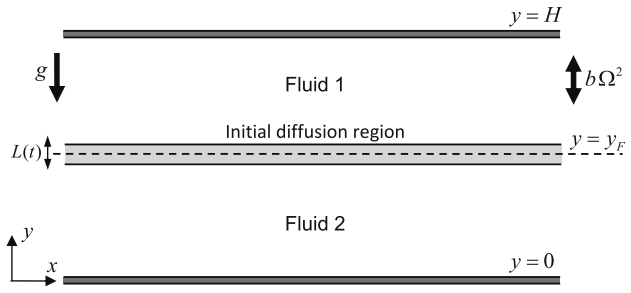


FIG. 1. Schematic of the fluid configuration.

where $D$ is the mass diffusion coefficient. Invoking a semi-infinite approximation, i.e., when $H/L(t) >> 1$, with $H$ being the total depth, the concentration field at early times is given as

$$\frac{C_0(y,t) - C_2}{\Delta C} = \frac{1 + erf\left((y - y_F)/2\sqrt{D\,t}\right)}{2}, \tag{2}$$

where $\Delta C = C_1 - C_2$; $C_1$ and $C_2$ are the concentrations of fluid "1" and fluid "2" and $y_F$ is the ordinate of the center of diffusion layer.

The primary objective of the current work is to characterise the stability of the mixing region for an imposed oscillation of angular frequency "Ω" (period $T = 2\pi/\Omega$) and amplitude "$b$". For this purpose, a Floquet-based linear stability analysis is carried out by invoking the Boussinesq approximation. In fact, the stability of the mixing layer is determined here by evaluating its response to the imposed oscillations at different time instants, $t_0$, of the quiescent base-state evolution. At each time, $t_0$, the base state for the linear analysis is given as $\mathbf{V}_0 = \{u_0, v_0, w_0\} = 0$ and $C_0$, where $C_0$ is obtained via Eq. (2). The difficulty in this approach arises from the temporal variation of concentration gradient in the base state making the resulting linear system of equations unsuitable for a classical Floquet type of analysis.

The current work remedies the above issue by using a quasi-static (frozen-field) approach, wherein the evolving base concentration field at time, $t_0$, is considered to remain frozen during the growth/decay of perturbations, i.e., $\partial C_0/\partial t = 0$, noting that $t$ is not the same as $t_0$. Such an approach effectively eliminates all the non-harmonic components of evolution from the linear analysis and is justifiable when the time constant of mass transfer, $t_0$, is much greater than the period of parametric forcing, $T$. As the rate of species diffusion is inversely related to the time, $t_0$, the term $\partial C_0/\partial t$ can be considered insignificant at higher $t_0$. Nevertheless, it would be beneficial to bring out plausible results at $t_0$ values as low as possible, i.e., for thin diffusion layers. As the concentration gradient, $\partial C_0/\partial y$, is the driving force behind the evolution of miscible Faraday instability, it is essential to consider thin layers as they provide enhanced mixing at lower threshold values.

For all situations considered in this study, the frozen thickness $L(t_0)$ of the mixing region is much smaller than the actual fluid depths ($H$). Thus, it becomes an apt reference length scale for the miscible fluid systems under consideration, i.e., $L_{ref} = \sqrt{Dt_0}$. While $T$ is chosen as the reference time scale here, i.e., $t_{ref} = T$, the other relevant scales are given as follows: velocity scale, $v_{ref} = \sqrt{Dt_0}/T$; pressure scale, $p_{ref} = \rho_0 D\,\nu/L_{ref}^2$; concentration scale, $\Delta C$. The density distribution in the domain is given as $\rho = \rho_0 - \rho_0\beta_c\,(C - C_2)$, where $\beta_c$ is the solutal expansion coefficient, $\beta_c > 0$. Owing to the Boussinesq approximation, the effect of density non-homogeneity is considered to be significant only in the buoyancy term of the Navier-Stokes equation. The scaled dimensionless mass, momentum, and species conservation equations in the oscillating reference frame are written as

$$\begin{gathered}\nabla\cdot\mathbf{V} = 0,\\ \frac{1}{Sc}\left[\frac{\partial\mathbf{V}}{\partial t} + (\mathbf{V}\cdot\nabla)\,\mathbf{V}\right] = -\frac{1}{t_0^{*2}}\nabla p + \frac{1}{t_0^{*}}\nabla^2\mathbf{V} + \frac{1}{t_0^{*2}}Ra\,(t)\;C\,\widehat{j}, \quad \text{and}\\ \frac{\partial C}{\partial t} + (\mathbf{V}\cdot\nabla)\,C = \frac{1}{t_0^{*}}\nabla^2 C.\end{gathered} \tag{3}$$

Here, $t_0^*$ is the ratio $t_0/T$, $Ra\,(t) = \beta_c\, a_{eff}\, \Delta C\, L_{ref}^3/D\,\nu$ is the solutal Rayleigh number, and $Sc = \nu/D$ is the Schmidt number. The effective acceleration $(a_{eff})$ acting on the fluids is given as $\{g + b\,\Omega^2 sin(W_0 t)\}\,\widehat{j}$, where $W_0$ is the Womersley number defined as $W_0 = \Omega\, t_{ref} = 2\pi$. No slip boundary conditions are imposed at the top and bottom plates, cf. Fig. 1.

With the temporal freezing of the base state, i.e., $\mathbf{V}_0 = 0$ and $C_0$, the evolution of any imposed infinitesimal perturbation, $(\mathbf{V}'; C')$, is governed by the linearised form of Eq. (3) written as

$$\nabla \cdot \mathbf{V}' = 0, \tag{4}$$

$$\frac{1}{Sc}\frac{\partial \mathbf{V}'}{\partial t} = -\frac{1}{t_0^{*2}}\nabla p' + \frac{1}{t_0^*}\nabla^2 \mathbf{V}' + \frac{1}{t_0^{*2}} Ra\,(t)\, C'\,\widehat{j}, \quad \text{and} \tag{5}$$

$$\frac{\partial C'}{\partial t} + v'\frac{\partial C_0}{\partial y} = \frac{1}{t_0^*}\nabla^2 C'. \tag{6}$$

The base concentration derivative, $\partial C_0/\partial y$, in the above equation is obtained by differentiating Eq. (2) and scaling it with $L_{ref}$ corresponding to each chosen $t_0$, i.e.,

$$\frac{\partial C_0}{\partial y} = \frac{1}{2\sqrt{\pi}} e^{\{-(y-y_F)^2/4\}}. \tag{7}$$

Now, on eliminating the horizontal components of velocities and pressure by operating Eq. (5) with $\widehat{j}\cdot\nabla\times\nabla\times$ and then by recombining with Eq. (4), we obtain

$$\left(\frac{1}{Sc}\frac{\partial}{\partial t} - \frac{1}{t_0^*}\nabla^2\right)\nabla^2 v' = \frac{1}{t_0^{*2}} Ra\,(t)\,\nabla_H^2 C' \text{ and} \tag{8}$$

$$\left(\frac{\partial}{\partial t} - \frac{1}{t_0^*}\nabla^2\right) C' = -v'\frac{\partial C_0}{\partial y}. \tag{9}$$

Here, $\nabla_H^2 = \partial^2/\partial x^2 + \partial^2/\partial z^2$. With suitable manipulations, it can be shown that Eqs. (8) and (9) can be written in a simplified form as

$$\frac{d\mathbf{X}'}{dt} = A(t)\,\mathbf{X}', \tag{10}$$

where $\mathbf{X}' = \{v', C'\}^T$ and $A(t)$ is the $T$-periodic linear operator corresponding to Eqs. (8) and (9). It is only due to the assumption of a frozen base state that the matrix $A(t)$ is $T$-periodic and the system of equations given by Eq. (10) is of the Floquet type. Its solution is represented as $\mathbf{X}' = e^{\mu t}\tilde{\mathbf{X}}$, where $\mu = \sigma + i\alpha$ is the Floquet exponent and $\tilde{\mathbf{X}}$ is the $T$-periodic Floquet mode. Here, $\sigma$ is assumed to be real and the value of $\alpha$ is either "0" for harmonic responses or "$\pi$" for sub-harmonic responses.[11] Upon further expansion of $\tilde{\mathbf{X}}$ in terms of a periodic series with fundamental frequency $2\pi$, $\mathbf{X}'$ may be written as

$$\mathbf{X}' = e^{\mu t}\sum_{n=-\infty}^{\infty}\widehat{\mathbf{X}}_n e^{i2n\pi t}. \tag{11}$$

In the current problem where the geometry is of infinite horizontal extent, $\widehat{\mathbf{X}}$ can be re-expanded in horizontal Fourier modes to give

$$\{v', C'\} = e^{\mu t}\sum_{n=-\infty}^{\infty}\{\widehat{v}_n(y), \widehat{C}_n(y)\}e^{i(k_x x + k_z z)}e^{i2n\pi t}, \tag{12}$$

where $k_x$ and $k_z$ are the wavenumbers in the horizontal directions $x$ and $z$, respectively. The solutal Rayleigh number, $Ra(t)$, is decomposed into static and vibrational components as $Ra\,(t) = Ra_s + Ra_v sin\,(2\pi t)$, where $Ra_s = \beta_c\, g\,\Delta C\, L_{ref}^3/D\,\nu$ and $Ra_v = \beta_c\, b\,\Omega^2\,\Delta C\, L_{ref}^3/D\,\nu$. Substituting the expansions of $v'$ and $C'$ from Eq. (12) into Eqs. (8) and (9), the perturbation equations for each periodic mode "$n$" are written as follows:

$$\frac{B_n}{Sc}\left(\frac{d^2}{dy^2} - k^2\right)\widehat{v}_n - \frac{1}{t_0^*}\left(\frac{d^2}{dy^2} - k^2\right)^2\widehat{v}_n = -\frac{k^2 Ra_s}{t_0^{*2}}\widehat{C}_n - \frac{i\,Ra_v k^2}{2\,t_0^{*2}}\left(\widehat{C}_{n+1} - \widehat{C}_{n-1}\right) \text{ and} \tag{13}$$

$$B_n\widehat{C}_n - \frac{1}{t_0^*}\left(\frac{d^2}{dy^2} - k^2\right)\widehat{C}_n = -\frac{\partial C_0}{\partial y}\,\widehat{v}_n. \tag{14}$$

Here, $B_n = i\,(\alpha + 2n\pi)$ and $k^2 = k_x^2 + k_z^2$. Since the current focus is to primarily predict the neutral behaviour, $\sigma$ is set to be zero. The reality conditions associated with the harmonic and sub-harmonic modes are given as

$$\widehat{C}_{-1} = \widehat{C}_1^* \qquad (harmonic\ mode, \alpha = 0), \tag{15}$$

$$\widehat{C}_{-1} = \widehat{C}_0^* \qquad (sub\text{-}harmonic\ mode, \alpha = \pi), \tag{16}$$

where "*" indicates complex conjugate.

The boundary conditions corresponding to no-slip plates at the impermeable top and bottom walls are as follows:

$$\widehat{v}_n = 0,\ \frac{d\widehat{v}_n}{dy} = 0,\ \frac{d\widehat{C}_n}{dy} = 0. \tag{17}$$

Note that the concentration perturbations at the top and bottom walls are specified here with Neumann conditions. Under the present semi-infinite distance approximation for the base-state, i.e., $L_{ref}/H << 1$, the results are not very sensitive to the type of boundary conditions applied at the walls.

The last step before the factorization of Eqs. (13) and (14) is the spatial discretization of variables in the $y$-direction for evaluating their respective derivatives. In this regard, a very accurate representation is generally possible with the use of Lagrangian interpolation polynomials defined over the G-L-C points. The distribution of G-L-C points is given by $y_j = \cos\left(\frac{\pi j}{N}\right)\ \{j = 0, 1, \ldots, N\}$, where $N$ is the number of collocation points considered along the $y$ direction. Whence, any unknown variable $\varphi$ is interpolated from its nodal values as

$$\varphi_N(y) = \sum_{j=0}^{N} h_j(y)\,\varphi(y_j), \tag{18}$$

where the function $h_j(y)$ is defined over the G–L–C points as follows:

$$h_j(y) = \frac{(-1)^{j+1}\left(1 - y^2\right)T_N'(y)}{\bar{c}_j N^2\left(y - y_j\right)}, \quad j = 0, 1, \ldots, N. \tag{19}$$

Here, $T_N'(y)$ corresponds to the first derivative of the $N^{th}$ Chebyshev polynomial of the first kind. The constant $\bar{c}_j$ is unity for all $j$ except at the extremities ($j = 0\,\&\,N$) where its value is 2. Any spatial derivative of $\varphi$ at the G-L-C points is subsequently obtained by differentiating Eq. (18) with the additional consideration of discrete orthogonality, i.e., $h_i(y_j) = \delta_{ij}$.

Unfortunately, a direct implementation of the above procedure does not suffice for the configuration of miscible fluid systems under study. Owing to the distribution pattern of G-L-C points (finer in the extremities and coarser in the center), the diffusion region in the middle of the domain is not well-resolved. In fact, in most situations, the thin diffusion layer is populated only by a single G-L-C point at its center and so, the actual error function profile of the species concentration is very poorly approximated. The resulting error in evaluating the corresponding sharp gradient leads to inaccurate predictions of the criticality. Any remedial clustering of nodes, using arbitrary points other than G-L-C points around the mixing region does not actually improve the accuracy of predictions, as the polynomial interpolation using such nodes results in the Runge phenomenon.[12]

One of the possible ways of overcoming this issue, i.e., the Runge phenomenon, involves a mapping strategy, wherein the actual polynomial interpolation is carried out only in the transformed coordinates ($\eta$). In the physical domain ($y$), the nodes are conveniently clustered around the diffusion region for an effective representation. Subsequently, these nodes are mapped onto the G-L-C points in the transformed domain ($\eta$) using suitable conformal mapping relations, $y = g(\eta)$. A candidate[13] that has been used in the present work for the purpose of transformation, cf. Fig. 2, is

$$y = g(\eta) = \epsilon \sinh\left\{\eta \sinh^{-1}(1/\epsilon)\right\}, \tag{20}$$

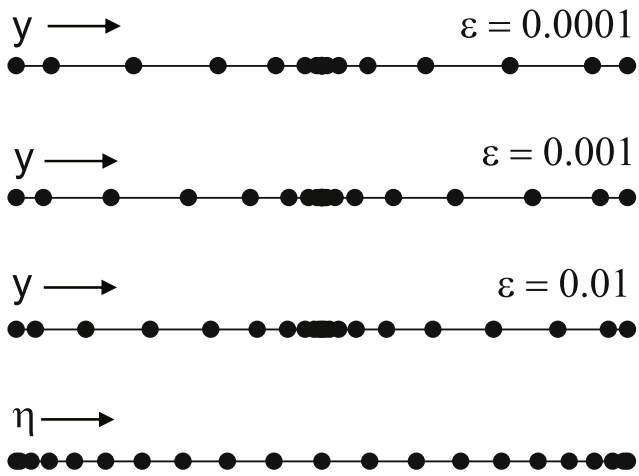


FIG. 2. Mapping of clustered node points ($y$) onto G-L-C points ($\eta$) in the transformed domain.

where $\epsilon$ is a scaling factor which determines the redistribution pattern of nodes in the physical domain. As evident from Fig. 2, the nodes are more densely packed around the central region as the value of $\epsilon$ gets lower. In view of the above mapping (Eq. (20)), the resulting transformations of all the spatial derivatives in Eqs. (13) and (14) are listed in the Appendix.

Following the transformation of all the spatial derivatives, the resulting set of equations can be written as a generalized eigenvalue problem of the form $\underline{\underline{M}}X = Ra_v\underline{\underline{N}}X$. In an experiment, the input parameters are the thermo-physical properties, layer heights, the initial waiting time, $t_0$, and the frequency of shaking. In dimensionless terms, the input parameters are $Ra_s$, $Sc$, $t_0^*$, and $y_F$. The key output parameter is the critical amplitude of shaking and in dimensionless terms, it is the critical value of $Ra_v$.

Before obtaining the critical conditions for the problem under study, the numerical method is verified by solving the vibrational Rayleigh-Bénard problem where the base-state profile is linear and the solutal problem is replaced by its thermal analog. Figure 3 shows the comparison of neutral curves obtained from the current implementation with the work of Shukla and Narayanan.[6] The present results have been obtained using the parameters $n_{max} = 8$ (total number of periodic modes considered), $N = 64$, and $\epsilon = 0.01$. Owing to the constant gradient of the base-state temperature, the results obtained are not very sensitive to these parameters. However, it will be soon shown that their values are important in obtaining accurate solutions for miscible Faraday systems. As evident from Fig. 3, an excellent match of our results with those of Shukla and Narayanan is observed for different Rayleigh numbers and heating configurations. The fundamental mode of excitation for the bottom heating case is harmonic, whereas for the top heating case, it is sub-harmonic.

Having verified the procedure with the special case of a constant gradient, it is now important to determine the optimum values of parameters, $N$ and $\epsilon$, that must be used for all the current computations related to miscible Faraday instability. As the goal of the mapping procedure is to accurately resolve the mixing region between the two fluids, these optimum values are best determined at the moment when the diffusion layer is the thinnest. It may be noted that the thinnest layer that can be considered in the current analysis is limited by the quasi-steady approximation according to which $t_0$ should be greater than $T$, i.e., $t_0^* >> 1$ and hence, an optimization study is carried out for $t_0 = 100$ s. The set of parameters thus identified would be even more appropriate at higher $t_0$ as the corresponding diffusion layer will be proportionally thicker. Here, the critical parameter of instability onset is represented by the ratio between the vibrational and static Rayleigh numbers, $Ra_v/Ra_s$ or simply $b\Omega^2/g$. This group ensures that the results are independent of the various fluid properties involved.

Figure 4(a) shows the variation of calculated $b\Omega^2/g$ values for different combinations of $N$ and $\epsilon$, for other relevant properties being $Ra_s = 10^5$, $D = 10^{-9}$ m$^2$/s, $Sc = 1000$, $t_0^* = 400$ ($t_0 = 100$ s

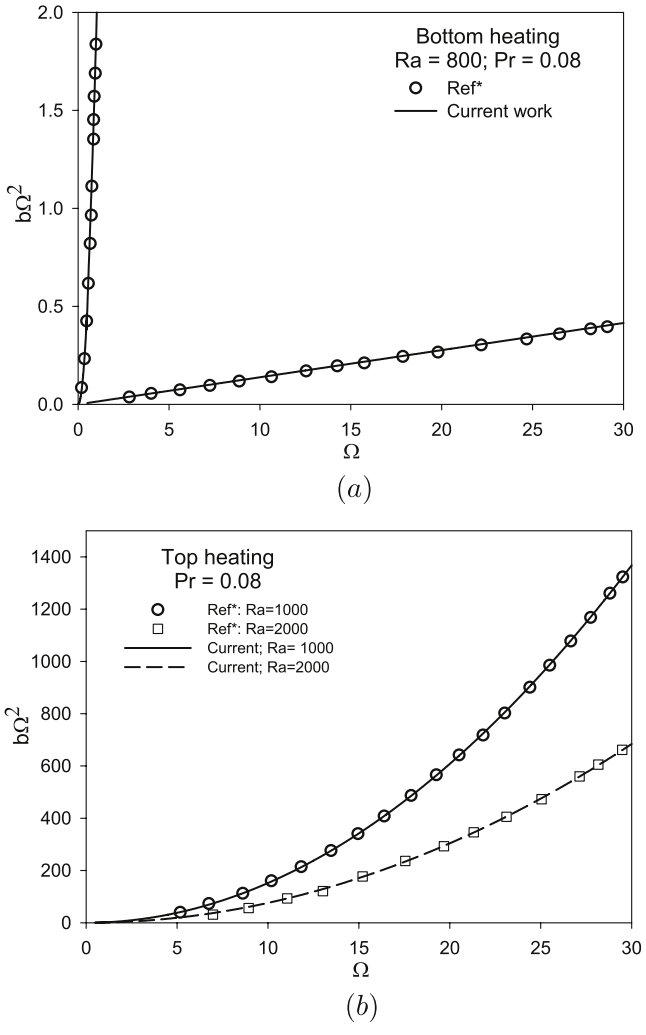


FIG. 3. Comparison of neutral curves obtained for thermo-vibrational convection: (a) bottom heating and (b) top heating (Ref* - Shukla and Narayanan[6]). Here, $Ra = \beta\, g\, \Delta\theta\, L_{ref}^3/\kappa\,\nu$ is the thermal Rayleigh number and $Pr = \nu/\kappa$ is the Prandtl number, with $\beta$ and $\kappa$ being thermal expansion coefficient and thermal diffusivity, respectively.

and $T = 0.25$ s), and $k^2 = \pi^2/2$. As seen, the $b\Omega^2/g$ values are observed to be strongly dependent on the scaling factor $\epsilon$ which determines the amount of grid-point clustering around the diffuse interface. For values of $\epsilon$ greater than $1/1000$, the convergence rate of $b\Omega^2/g$ with $N$ is observed to vary inversely with $\epsilon$. At values of $\epsilon$ lesser than or equal to $1/1000$, the predicted $b\Omega^2/g$ converges at nominal ranges of $N$, as the diffuse interface is now well resolved. However, with the further reduction of $\epsilon$ say to $1/10\,000$, the variation of $b\Omega^2/g$ with $N$ is observed to be initially oscillatory. Such behavior is not surprising as the condition number of the fourth-order differentiation matrix worsens with the increased proximity of the grid points around the mixing region.[14] In this regard, a value of $\epsilon = 1/2000$ is chosen here as it allows for a proper convergence at moderate values of $N$. In order to aid in deciding the optimum $N$ value, the distances of the first, second, and third grid points from the domain center for each of the mapping parameters are plotted in Figs. 4(b)–4(d). The horizontal guideline in these figures corresponds to $L_{ref}$ which in turn represents the thickness of the diffusion layer. The utility of this guideline is to facilitate the estimation of number of grid points that will populate the diffuse interface for each parametric case. As seen, at $\epsilon = 1/2000$, the diffuse interface is well resolved for values of $N$ upward of 72 and so an accurate estimate of gradients can be expected beyond $N = 72$. However, for the sake of optimizing the associated computational effort, all the computations in the present work have

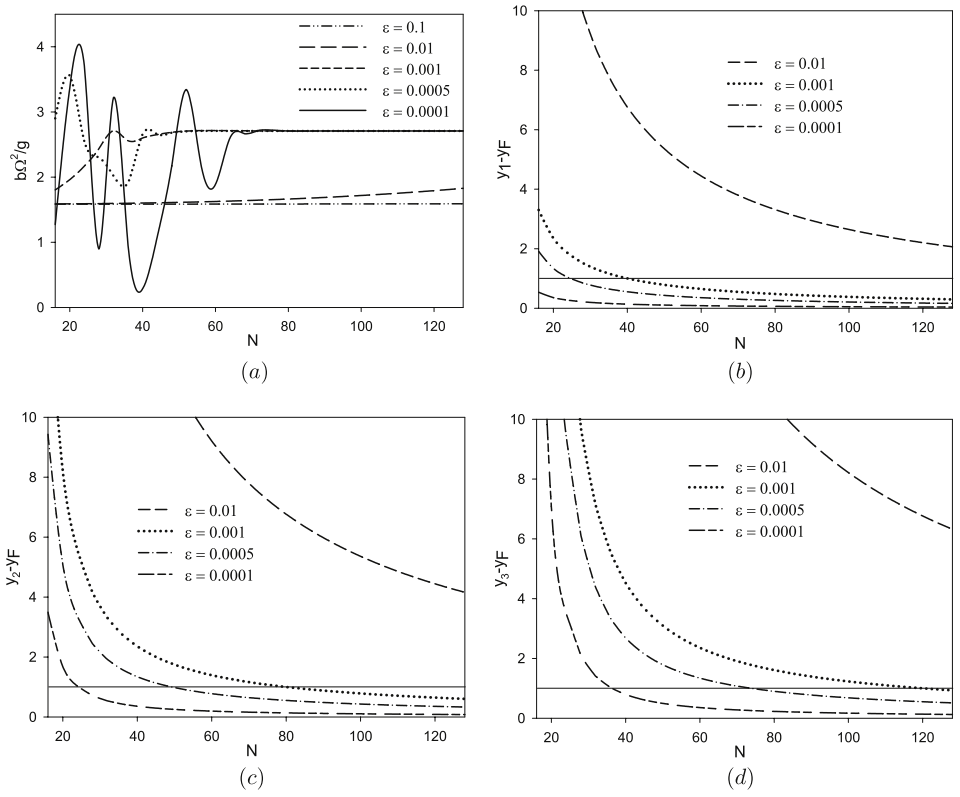


FIG. 4. Influence of parameters $\epsilon$ and $N$ on (a) acceleration ratio, (b) first, (c) second, and (d) third grid points from the center. $Ra_s = 10^5$, $t_0^* = 400$, $Sc = 1000$, $D = 10^{-9}$ m$^2$/s, and $k^2 = \pi^2/2$.

been carried out at $N = 72$ and $\epsilon = 1/2000$. The value of parameter, $n_{max}$, has been chosen to be 6 for all computations as any further increase in its value does not result in a tangible change of critical $Ra_v$.

## III. RESULTS

The determination of the Faraday instability threshold in miscible fluid systems involves several dimensionless groups. In order to understand the physics of the instability from the calculations, we shall contain ourselves to a specific fluid system, in this case, the brine/water system. This miscible fluid pair is chosen because the thermophysical properties are well documented and the system was experimentally investigated by Zoueshtiagh *et al*.[3] As noted earlier, once the fluid system and layer heights have been chosen in an experiment, the other two input variables are the waiting time and the frequency of parametric forcing. The output is the critical amplitude at which the flow commences with a discernible wavelength. With this in mind, we shall proceed to show the dependence of the output amplitude, $b$, on the input frequency for fixed waiting times as well as the dependence of $b$ on the waiting time for fixed frequencies. An important by-product of the calculations is the critical wavenumber at which the instability manifests itself. The values of the kinematic viscosity and diffusion coefficient for the brine/water system give a Schmidt number, $Sc$, of the order of $10^3$. In all our calculations, we assume that the contact point between the two fluids is at the mid plane, i.e., $y_F$ (unscaled) = $H/2$, the concentration difference $\Delta C$ is taken to be 1, and the solutal expansion coefficient is of the order $1/10$.

Our first calculation depicts the harmonic and the sub-harmonic responses of the scaled critical amplitude with respect to the scaled wavenumber. As seen from Fig. 5, the fundamental excitation of the system here is sub-harmonic because the respective critical parameters are lower than the harmonic mode for all the values of wavenumber, $k$, considered. This behavior agrees with the

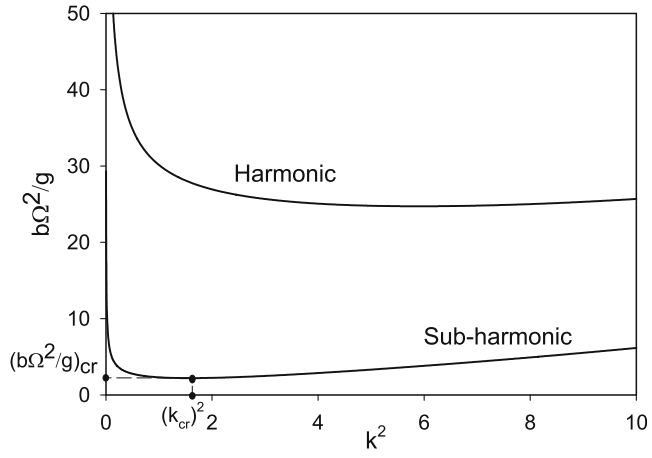


FIG. 5. Fundamental harmonic and sub-harmonic neutral curves obtained at $t_0 = 500$ s for a fluid system with $Ra_s = 10^5$, $Sc = 1000$, $y_F = 707$, and $t_0^* = 2000$.

experimental observations of Zoueshtiagh *et al*.[3] where the actual frequency of instability was found to be one half of the excitation frequency.

The criticality of the sub-harmonic mode also confirms the analogy between the miscible Faraday and the top-heated vibrational R-B systems. Similar to the latter, the minimum in the acceleration ratio occurs on account of distinct features observed at lower and higher values of wavenumbers. At low values of $k^2$, the transverse perturbations imposed on the layers are far apart and, hence, the density variations that drive the instability are also far apart. This necessitates a larger amplitude of oscillations for the onset of instability in the layers. At the same time, the predominance of viscous dissipation effects owing to choppy waves at large wavenumbers once again results in a higher critical amplitude of the imposed oscillations. Thus, a trade-off between these effects leads to a minimum in the acceleration ratio. For the fluid configuration under consideration, the critical values of acceleration ratio, $(b\Omega^2/g)_{cr}$, and wavenumber, $k_{cr}^2$, are 2.2 and 1.56, respectively. Observe that the critical wavelength is roughly the thickness of the solutal boundary layer, which is about five times $L_{ref}$ or $\sqrt{D\,t_0}$, a physically plausible result for the transient diffusion problem. It may be noted that for all the computations to follow, only the results corresponding to the fundamental sub-harmonic mode are presented.

Proceeding further, we shall now explain the variation of the critical amplitude with the frequency, both in unscaled and scaled terms. Figure 6(a) shows a rising value of $b$ with respect to $t_0^*$ for various waiting times. It may be noted here that an increase in $t_0^*$ for a fixed waiting time implies an increase in the forcing frequency. As the frequency approaches zero, the figure appears to show values of decreasing critical amplitude. However, we believe that at extremely small values of input frequencies, the critical amplitudes ought to rise and become unbounded. This region is not shown in the figure and, in fact, is a region where the frozen-time approach is invalid. The early rise of $b$ with $t_0^*$ can be understood from the fact that the critical wavenumber also increases with frequency or $t_0^*$, cf. Fig. 6(b). This implies that decreasing wavelengths or choppy modes are obtained with increasing frequency and this, of course, leads to viscous stabilization. The ultimate leveling-off of the amplitude is due to the fact that increasing input frequencies also imply increasing forcing acceleration and a decrease in the critical amplitude is necessary to thwart the destabilization that is caused by the increased acceleration. The last figure, Fig. 6(c), shows the variation of scaled amplitude change with $t_0^*$. For each $t_0$, though the unscaled critical amplitude actually begins to decay slowly beyond a $t_0^*$ value, a monotonic increase of the scaled amplitude occurs on account of increasing $\Omega^2$.

In order to see the dependence of the critical "$b$" with the wait time, the frequency is now held fixed and the wait time is varied. This dependence is depicted in Fig. 7. In such a calculation, parameters such as $Ra_s$ and scaled $y_F$ have to be varied as $t_0^*$ varies, because they directly depend on the wait time. It is thus convenient to write $Ra_s$ as $Ra_T(t_0^*)^{3/2}$, where $Ra_T = \beta_c\, g\, \Delta C\, (D\,T)^{3/2}/D\,\nu$.

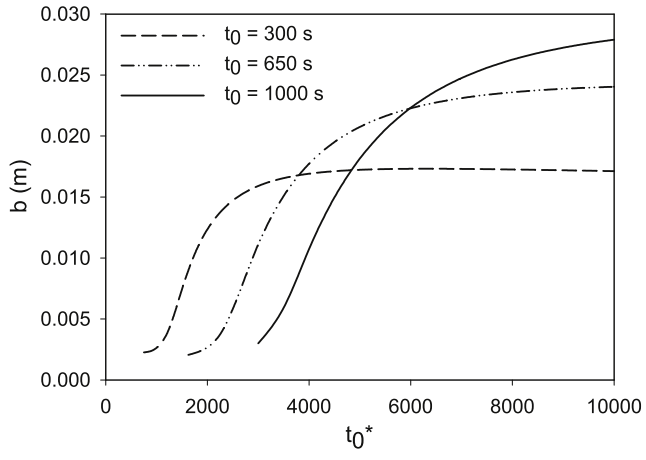


(*a*)

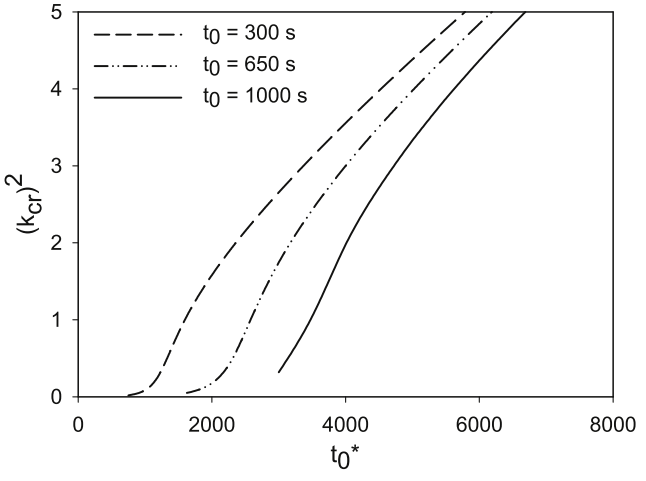


(*b*)

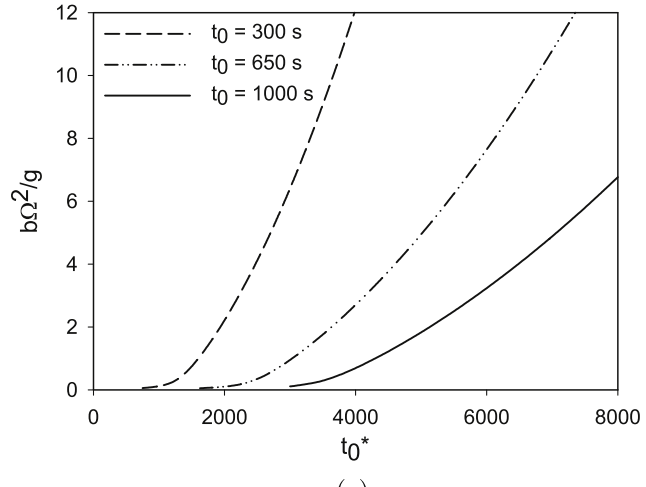


(*c*)

FIG. 6. Influence of $T$ for a fluid system with properties $D = 10^{-9}$ m$^2$/s and $Sc = 1000$ at $t_0 = 300$ s, 650 s, and $t_0 = 1000$ s. $Ra_s$ for each $t_0$ is given as $Ra_s = 10^5 \times (t_0/300)^{3/2}$. (a) Unscaled amplitude. (b) Critical wavenumber. (c) Critical acceleration ratio.

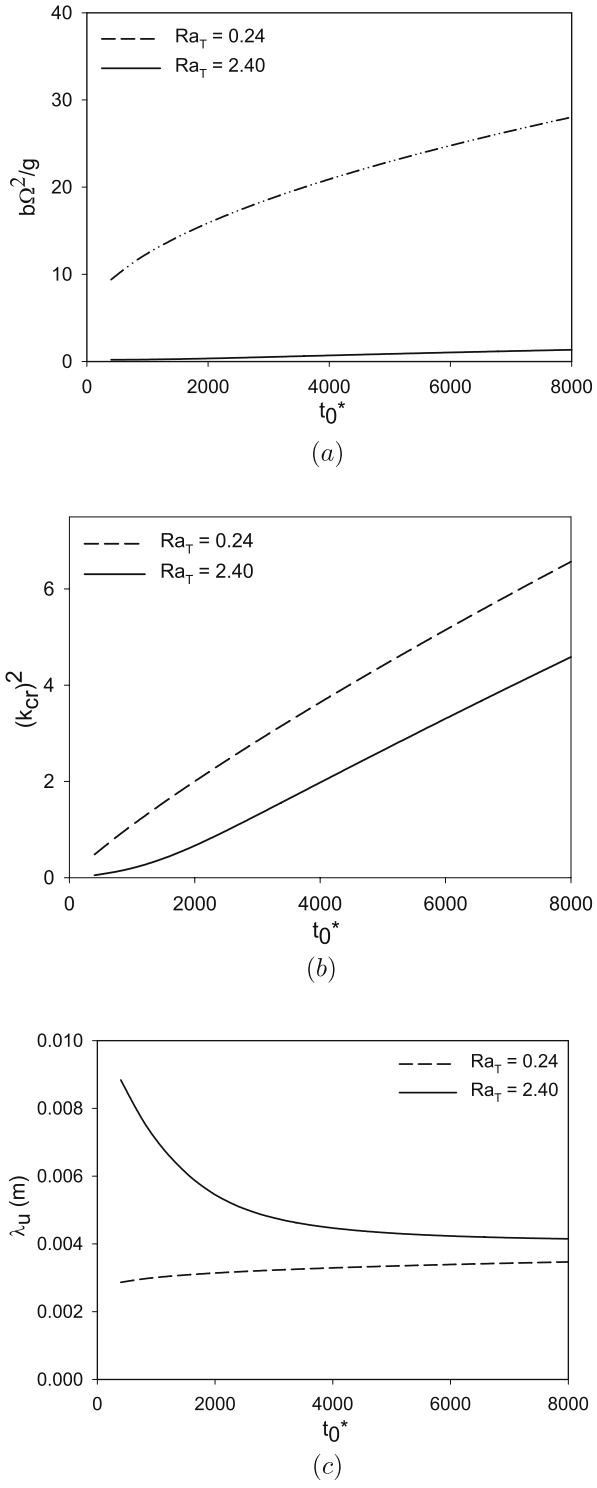


FIG. 7. Influence of $t_0$ for a fluid system with properties $D = 10^{-9}$ m$^2$/s, $Sc = 1000$, and $T = 0.25$ s. (a) Critical acceleration ratio. (b) Critical wavenumber. (c) Unscaled wavelength.

Figure 7 correspondingly shows the predicted variations of critical acceleration ratio and wavenumber with $t_0^*$ for two different values of $Ra_T$. The $Ra_T$ here brings in the effects of thermo-physical properties and also the fixed frequency of the imposed oscillation. In the present physical situation where both the layer thickness and $\partial C_0/\partial y$ are dependent on $t_0$, they have opposing influences

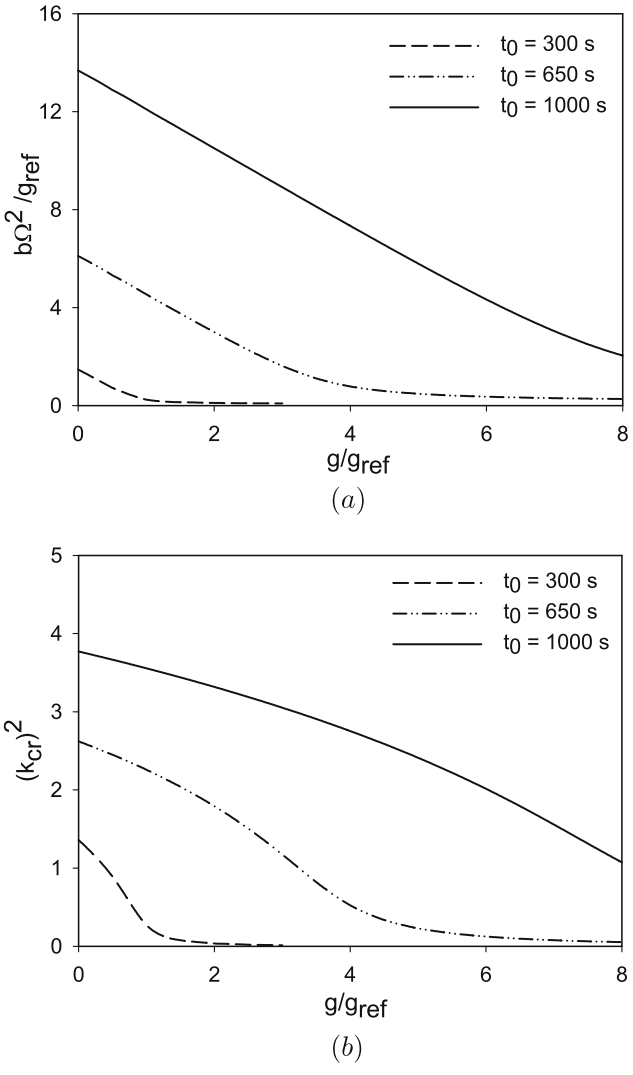


FIG. 8. Predicted influence of gravity on a fluid system with properties $D = 10^{-9}$ m$^2$/s and $Sc = 1000$. The time period of the imposed oscillation is $T = 0.25$ s. (a) Critical acceleration ratio. (b) Critical wavenumber.

on the stability of the layer. While the former is stabilizing at lower $t_0$, the latter is destabilizing owing to its large magnitude and the large value of the solutal expansion coefficient. With an increase in $t_0$, the magnitude of both these effects decreases. The monotonic increase of the neutral curve in Fig. 7(a) implies that the stabilizing effect brought in by the decreasing concentration gradient overwhelms the loss of stability due to increasing layer thickness. In other words, the reduction in vertical concentration gradient at higher values of $t_0$ matters more, so that an increase in the vibrational acceleration is required to induce the Faraday instability. This behavior has been experimentally observed by Zoueshtiagh *et al.*[3] for both their water/brine and oil/oil systems. It is be noted that the present variable $t_0$ has the same physical meaning as their experimental wait time.

As evident from Fig. 7(b), the critical wave number ($k$) of excitation monotonically increases with the increase of $t_0^*$. This might give an initial impression that the critical wavelength ($\lambda = 2\pi/k$) also decreases monotonically with $t_0$. However, as the reference length is a function of $t_0$ in the present case, the unscaled critical wavelength ($\lambda_u = \lambda L_{ref}$), as shown in Fig. 7(c), has a different pattern of variation as opposed to $\lambda$. As evident, the decrease or increase of critical wavelength, for the range of time duration studied, is determined by the thermo-physical properties of the fluid layers. For $Ra_T = 0.24$, a gradual increase is observed as opposed to a monotonic decrease for $Ra_T = 2.4$.

The latter behavior is similar to the experimental observation of Zoueshtiagh *et al.*[3] where a slow monotonic decrease has been observed for their brine/water system.

Finally, the effect of gravitational acceleration on the onset of miscible Faraday instability is now analyzed. This is achieved by gradually varying the $Ra_s$ of the fluid layer ($Sc$ = 1000 and $D = 10^{-9}$ m$^2$/s) at fixed values of $t_0$ and $T$ (=0.25 s). Considering a reference value of gravity, $g_{ref}$, for which the static Rayleigh number is $Ra_{ref}$ at a given $t_0$, the effect of gravity change, $g/g_{ref}$, can be measured through the ratio $Ra_s/Ra_{ref}$. The ratio of $b\Omega^2/g$ can be multiplied with $g/g_{ref}$ to obtain an independent output parameter, $b\Omega^2/g_{ref}$, for the problem. Figure 8(a) shows the corresponding neutral curves obtained for three different values of $t_0$ = 300 s, 650 s, and 1000 s. Surprisingly, for all the $t_0$ values considered, the critical acceleration ratio decreases with an increase in gravity. This destabilizing influence of gravity is counter-intuitive, as it is normal to expect an enhanced stratification, hence more stability, when the gravity acting on the layers is increased. The observed behavior can be reasoned by considering the analog of a simple pendulum, whose natural frequency is proportional to $\sqrt{g/l}$. Imagine that the whole pendulum along with its pivot is now subjected to vertical vibrations of a constant frequency. Consequently, the motion of the pendulum will be in tune with the frequency of the imposed oscillation. At this stage, any change in the gravitational acceleration acting on the pendulum mass must come attended with a corresponding change in the value of $l$, in order for the system to be in dynamic equilibrium with the imposed vibrations. Similarly, the act of changing the magnitude of gravity in the miscible Faraday problem must be accompanied with a change in critical wavelength of instability onset, for its response to be in-tune with the imposed oscillations. This behavior is exactly observed in Fig. 8(b) where the critical wavenumber undergoes a monotonic decrease with the increase in gravity. Since the dissipation effects associated with the long wavelength patterns are insignificant, the vibrational acceleration required for the onset of instability, in reality, reduces with the increase in gravity.

## IV. SUMMARY

A linear analysis of Faraday instability in miscible fluids has been carried out in the current work using Floquet theory in conjunction with a quasi-steady approximation. The field variables have been spatially discretised using spectral collocation, while the thin diffusion region between the layers has been well-resolved through a mapping strategy. The resulting eigenvalue problem yields the critical vibrational amplitude for different input parameters like wait time, frequency, and gravitational conditions.

The neutral behavior of the miscible Faraday system has been observed to be similar to that of the top-heated vibrational Rayleigh-Bénard problem. In all the cases considered, the criticality was observed to be sub-harmonic. The unscaled critical amplitude of vibration was found to initially increase with the imposed frequency. This is due to the stability brought in by the viscous dissipation associated with choppy waves. On account of increasing acceleration, the critical amplitude is observed to level-off at a particular frequency and slowly diminish thereafter. In situations where the imposed frequency is fixed and wait time is varied, the system is found to possess more stability at longer wait times. Though the effect of thin-layers is stabilizing, the associated concentration gradients make them highly vulnerable to instability. With an increase in layer thickness, the concentration gradient decreases and so, an enhanced stability is predicted. An analogy with a simple pendulum is used to explain why the predicted wavelength of the flow patterns increases with gravity. The associated reduction in viscous dissipation causes the layers to lose stability with an increase in gravity level.

A noteworthy aspect of the current work is that the analysis will not work at very low frequencies and low wait times. This may be overcome with the use of other methods involving "non-normal approach,"[15] which have the capability of resolving problems with an unsteady base state[16] like the present one. Notwithstanding this fact, the range of parameters studied in the work is valid for many practical purposes and hence, the present results are of immense value. Moreover, many of the results agree qualitatively with those of Zoueshthiagh *et al.*[3]

## ACKNOWLEDGMENTS

We acknowledge the support from the French Space Agency (CNES), the European Space Agency (ESA) topical team Liquid interfaces subjected to oscillations, and the Marie Curie International Research Staff Exchange Scheme (IRSES) Fellowship project titled Patterns and Surfaces (No. 269207). Also, support from NSF No. 0968313 is gratefully acknowledged.

## APPENDIX: TRANSFORMATION OF SPATIAL DERIVATIVES

With regard to the conformal mapping procedure adopted in Eq. (20), the spatial derivatives of any variable $\phi$ such as $\widehat{v}$ or $\widehat{C}$ are obtained through the following transformations:

$$\frac{d\phi}{dy} = \frac{1}{g'}\frac{d\phi}{d\eta}, \tag{A1}$$

$$\frac{d^2\phi}{dy^2} = \frac{1}{(g')^2}\frac{d^2\phi}{d\eta^2} - \frac{g''}{(g')^3}\frac{d\phi}{d\eta}, \tag{A2}$$

$$\frac{d^3\phi}{dy^3} = \frac{1}{(g')^3}\frac{d^3\phi}{d\eta^3} - \frac{3g''}{(g')^4}\frac{d^2\phi}{d\eta^2} - \frac{g'g''' - 3(g'')^2}{(g')^5}\frac{d\phi}{d\eta}, \text{and} \tag{A3}$$

$$\frac{d^4\phi}{dy^4} = \frac{1}{(g')^4}\frac{d^4\phi}{d\eta^4} - \frac{6g''}{(g')^5}\frac{d^3\phi}{d\eta^3} - \frac{4g'g''' - 15(g'')^2}{(g')^6}\frac{d^2\phi}{d\eta^2} - \frac{(g')^2g'''' - 10g'g''g''' + 15(g'')^3}{(g')^7}\frac{d\phi}{d\eta}. \tag{A4}$$

[1] M. Faraday, "On a peculiar class of acoustical figures; and on certain forms assumed by groups of particles upon vibrating elastic surfaces," Philos. Trans. R. Soc. London **121**, 299–340 (1831).
[2] T. B. Benjamin and F. Ursell, "The stability of the plane free surface of a liquid in vertical periodic motion," Proc. R. Soc. London, Ser. A **225**, 505–515 (1954).
[3] F. Zoueshtiagh, S. Amiroudine, and R. Narayanan, "Experimental and numerical study of miscible Faraday instability," J. Fluid Mech. **628**, 43 (2009).
[4] S. Amiroudine, F. Zoueshtiagh, and R. Narayanan, "Mixing generated by Faraday instability between miscible liquids," Phys. Rev. E **85**, 016326 (2012).
[5] P. Gresho and R. Sani, "The effects of gravity modulation on the stability of a heated fluid layer," J. Fluid Mech. **40**, 783–806 (1970).
[6] P. K. Shukla and R. Narayanan, "The effect of time-dependent gravity with multiple frequencies on the thermal convective stability of a fluid layer," Int. J. Heat Mass Transfer **45**, 4011–4020 (2002).
[7] V. Siddavaram and G. Homsy, "The effects of gravity modulation on fluid mixing. Part 1. Harmonic modulation," J. Fluid Mech. **562**, 445–475 (2006).
[8] Y. Gaponenko and V. Shevtsova, "Effects of vibrations on dynamics of miscible liquids," Acta Astronaut. **66**, 174–182 (2010).
[9] A. James, B. Vukasinovic, M. K. Smith, and A. Glezer, "Vibration-induced drop atomization and bursting," J. Fluid Mech. **476**, 1–28 (2003).
[10] A. Riaz, M. Hesse, H. Tchelepi, and F. Orr, "Onset of convection in a gravitationally unstable diffusive boundary layer in porous media," J. Fluid Mech. **548**, 87–111 (2006).
[11] K. Kumar and L. S. Tuckerman, "Parametric instability of the interface between two fluids," J. Fluid Mech. **279**, 49–68 (1994).
[12] J. P. Boyd, *Chebyshev and Fourier Spectral Methods* (Courier Dover Publications, 2001).
[13] T. W. Tee and L. N. Trefethen, "A rational spectral collocation method with adaptively transformed Chebyshev grid points," J. Sci. Comput. **28**, 1798–1811 (2006).
[14] L. Cueto-Felgueroso and R. Juanes, "Adaptive rational spectral methods for the linear stability analysis of nonlinear fourth-order problems," J. Comput. Phys. **228**, 6536–6552 (2009).
[15] P. Schmidt and D. Henningson, *Stability and Transition in Fluid Flows* (Springer, 2001).
[16] F. Doumenc, T. Boeck, B. Guerrier, and M. Rossi, "Transient Rayleigh–Bénard–Marangoni convection due to evaporation: A linear non-normal stability analysis," J. Fluid Mech. **648**, 521–539 (2010).